Available online at www.sciencedirect.com

ScienceDirect

Geochimica et Cosmochimica Acta 278 (2020) 261–271

Geochimica et Cosmochimica Acta

www.elsevier.com/locate/gca

Potassium isotope fractionation during continental weathering and implications for global K isotopic balance

Fang-Zhen Teng [a,*], Yan Hu [a], Jin-Long Ma [b], Gang-Jian Wei [b], Roberta L. Rudnick [c]

[a] Isotope Laboratory, Department of Earth and Space Sciences, University of Washington, Seattle, WA 98195, USA
[b] State Key Laboratory of Isotope Geochemistry, Guangzhou Institute of Geochemistry, Chinese Academy of Sciences, Guangzhou 510640, China
[c] Department of Earth Science and Earth Research Institute, University of California, Santa Barbara, CA 93106, USA

Received 13 December 2018; accepted in revised form 22 February 2020; available online 2 March 2020

Abstract

Potassium isotopic compositions of profiles through saprolites developed on a diabase in South Carolina, U.S.A., and on a granite in Guangdong, China, allow characterization of the behavior of K isotopes during continental weathering. Saprolites from the diabase profile are heavily weathered with chemical index of alteration (CIA) values up to 95; however, their K isotopic variation is limited, with $\delta^{41}K$ ranging from $-0.475 \pm 0.028‰$ in the unweathered diabase to $-0.407 \pm 0.021‰$ for the saprolites. The lack of significant K isotope fractionation mainly reflects the conservative behavior of K in the diabase weathering profile, with >50% of the original K remaining in the saprolites. By contrast, K isotopes are fractionated during granite weathering and correlate with sample depth, CIA, and kaolinite abundance, with $\delta^{41}K$ decreasing from $-0.493 \pm 0.030‰$ in the unweathered granites at the bottom to $-0.628 \pm 0.021‰$ in the most weathered saprolite close to the surface. These observations suggest the preference of light K isotopes in saprolites relative to fluids, which is further supported by the overall isotopically heavy nearby stream water samples ($\delta^{41}K = -0.709 \pm 0.017$ to $-0.339 \pm 0.018‰$). These results demonstrate that continental weathering plays an important role in the global K isotopic budget through the formation of isotopically heterogeneous rivers and weathered regolith. Recycling of K-rich crustal materials with distinct K isotopic signatures may produce distinct mantle K isotopic end members.

Keywords: Potassium isotopes; Continental weathering; Granite; Diabase; Global potassium cycle

1. INTRODUCTION

Continental weathering is the first and one of the key steps in global elemental cycling (Goldich, 1938). It releases elements from the continental crust into air, plants, and rivers for a trip to the oceans. Weathering drives the chemical evolution of the atmosphere, biosphere, hydrosphere, and continents over geologic time-scales (Brantley et al., 2011; Berner and Berner, 2012).

Continental weathering exerts a primary control on global isotopic budgets; it commonly produces large isotope fractionations that ultimately leads to the formation of distinct isotopic reservoirs (Valley and Cole, 2001; Teng et al., 2017). For example, chemical weathering shifts the isotopic composition of the hydrosphere and continents away from that of the mantle (e.g., Li and Mg isotopes, Penniston-Dorland et al., 2017; Teng, 2017), which lays the foundation for using stable isotopes as tracers of crustal cycling (Teng et al., 2019).

Recent development of K isotope geochemistry has documented large K isotopic variations (up to 2‰) that greatly exceed analytical precision (<±0.06‰, 2σ) in terrestrial rocks (Wang and Jacobsen, 2016a, 2016b; Li et al., 2016,

* Corresponding author.
E-mail address: fteng@u.washington.edu (F.-Z. Teng).

https://doi.org/10.1016/j.gca.2020.02.029
0016-7037/

2017; Parendo et al., 2017; Hu et al., 2018; Morgan et al., 2018; Chen et al., 2019a, 2019b; S.L. Li et al., 2019; Tuller-Ross et al., 2019; Xu et al., 2019; Huang et al., 2020; Sun et al., 2020). These studies indicate that the hydrosphere, especially seawater, has a homogenous and overall heavy K isotopic composition (Hille et al., 2019), whereas continental crustal rocks have highly heterogeneous and, on average, light K isotopic compositions (Huang et al., 2020). This large (~0.6‰) K isotopic difference between seawater and continental crust may reflect the influence of chemical weathering by analogy to other stable isotopes (e.g., Li and Mg isotopes, Penniston-Dorland et al., 2017; Teng, 2017). However, to date, few studies have been carried out to study the behavior of K isotopes during chemical weathering (S.L. Li et al., 2019; Huang et al., 2020).

Potassium is a major element in rivers (average K = 0.78 ppm) (Gaillardet et al., 1999) and continental crust (average K_2O = 1.81 wt%), particularly in the upper crust (average K_2O = 2.8 wt%) (Rudnick and Gao, 2003). Granite, among all types of crustal rocks, is the most common K-rich rock and dominates the K budget of the upper continental crust (Wedepohl, 1995). Therefore, studies of chemical weathering of granite, a main source of K in the hydrosphere, are essential for understanding K isotopic distribution and transport between the hydrosphere and continents, which places fudamental constraints on the global K isotopic budget.

Here we report high-precision K isotopic data for saprolites and related stream waters in a well-characterized, 40-meter weathering profile developed on granite in the tropical environment of Guangdong, South China. To assess the potential influence of protolith composition on K isotope fractionation, we also studied a well-characterized weathering profile developed on a diabase dike in the subtropical environment of South Carolina, U.S.A. We found limited K isotope fractionation during diabase weathering and significant fractionation during granite weathering, mainly reflecting their different degrees of K loss and different types of protoliths. These observations provide the first direct evidence for the preferential release of heavy K to the hydrosphere and the retention of isotopically light K in the continental regolith. They further suggest that continental weathering has a major control on the global K isotopic budget by producing the isotopically heterogeneous hydrosphere and continental crust.

2. SAMPLES

2.1. Granite weathering profile, Guangdong

The Fogang granite formed between 190 and 150 Ma and is located in Guangdong, South China (23°42′28.8″N, 113°30′14.4″E) in a tropical climate, with a mean annual temperature of ~25 °C and annual precipitation of 800 to 2500 mm (Wang et al., 2018). The granite weathering profile is located on a local hilltop ~28 m above the surrounding landscape. At the foot of this hill, a stream flows from east to west.

To avoid samples that are significantly influenced by biological activity, the top 1.5 m of the soil was discarded and the underlying weathering profile was drilled 40 m downwards until relatively unweathered parental rock was reached (Fig. 1). The bottom section of the profile from 39.8 to 31.6 m is the relatively unweathered granite, containing significant amounts of biotite (7.7%) and chlorite (7.2%) in addition to quartz (25.6%), K-feldspar (30.7%), and plagioclase (30.9%) (Wang et al., 2018). Towards the surface, weathering intensity gradually increases. Biotite and chlorite break down first and completely disappear at 30 m depth, followed by plagioclase that is completely decomposed at 25 m depth. Due to the dissolution of these minerals, the relative abundance of K-feldspar roughly increases until 10 m depth, and subsequently decreases upwards within the top 10 m of the profile. Secondary minerals (e.g., kaolinite and illite) start forming at about 25 m depth and continue upwards through the whole profile (Fig. 1). Among primary and secondary minerals, kaolinite is the most suitable mineral index for weathering intensity as it is the dominant secondary mineral; its abundance increases systematically upwards as the intensity of weathering increases (Fig. 1).

These mineralogical changes are also reflected in the chemical variations along the weathering profile, e.g., MgO and CaO contents decrease dramatically in the initial stage of weathering, reflecting the dissolution of mafic minerals and plagioclase (Wang et al., 2018). The K_2O concentration increases with the abundance of K-feldspar, and to a lesser extent, illite, in the weathering profile (Fig. 2). This is consistent with the fact that mineral-bound K is partially released into solution during weathering and that K-feldspar and illite are the major mineral hosts for K during granite weathering.

Eight stream water samples were collected at the base of the hill at different times over a year. They were filtered through 0.45 μm Millipore membrane filters in the field, and acidified immediately to pH < 2 using distilled nitric acid and then stored in polyethylene plastic bottles (Wang et al., 2018).

2.2. Diabase weathering profile, South Carolina

The diabase weathering profile formed during the Paleogene in a humid, subtropical climate on a diabase dike in South Carolina, U.S.A. (33°58′09″N, 81°3′7″W) (Gardner et al., 1981). Unweathered diabase contains significant amounts of talc (20%) and chlorite (8%), in addition to plagioclase (40%), clinopyroxene (29%), and opaque minerals (3%) (Gardner et al., 1981). Saprolite samples were collected along a 11 m vertical profile through the center of the dike (Fig. 3). As the intensity of weathering increases towards the surface, talc and chlorite were weathered first, followed by clinopyroxene and plagioclase (Gardner et al., 1981). Kaolinite, smectite, and Fe-oxides are the main weathering products (Gardner et al., 1981). At a depth of ~2 m a discontinuity is recorded in the clay mineralogy and chemical composition (Gardner and Kheoruenromne, 1980; Gardner et al., 1981). This

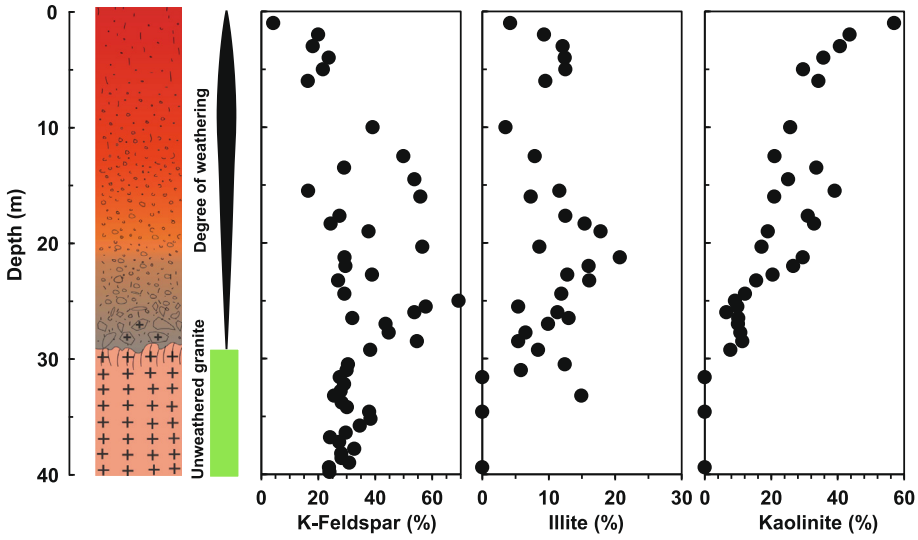

Fig. 1. Sketch of cross-section of the granite weathering profile (modified from Wang et al., 2018) and variations in key mineral abundances along the profile, with relatively unweathered granite at the bottom and an increasing degree of weathering upwards. Data in this and the following figures are reported in Tables 1–3.

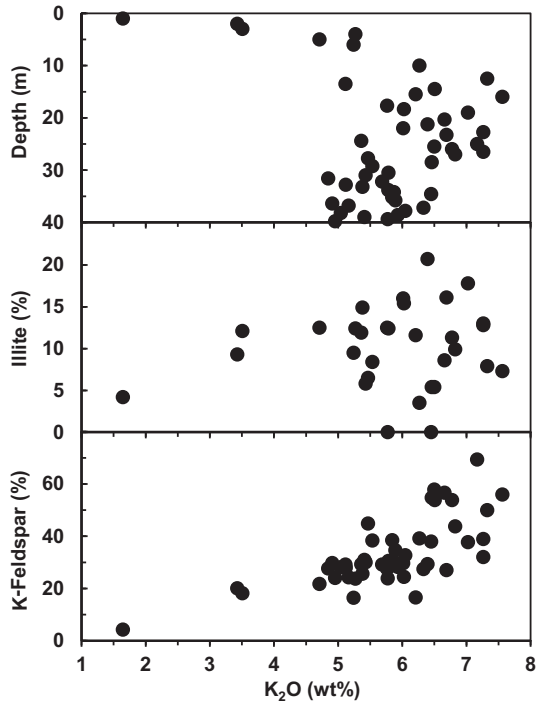

Fig. 2. Variation of K_2O content with depth, illite, and K-feldspar abundances in the granite weathering profile.

discontinuity was interpreted to reflect a change in redox, with the upper profile being more oxidized and lacking siderite, and the lower portion being more reduced and containing siderite.

The weathering intensity recorded by the saprolites increases upwards, as indicated by increasingly lower density, higher CIA (chemical index of alteration, see Table 1 for definition) values (up to 95) and large isotopic variations in Li, Mg, Cu, and Fe (Gardner et al., 1981; Rudnick et al., 2004; Teng et al., 2010; Liu et al., 2014). Compared to other major elements (e.g., Al, Fe, Ca, and Mg), the K_2O concentrations show smaller variations and are equal to or higher in saprolites than in the unweathered diabase (Fig. 3) (Gardner et al., 1981).

Nine saprolite samples from the weathering profile below the 2 m discontinuity and one unweathered diabase from 30 m depth were analyzed for K isotopes. Archived samples are not available above the discontinuity and, therefore, not analyzed here.

3. ANALYTICAL METHODS

The rock powders and stream waters investigated here are the same as those used in previous studies for characterizing their mineralogical, elemental and isotopic compositions (Gardner et al., 1981; Rudnick et al., 2004; Teng et al., 2010; Liu et al., 2014; Wang et al., 2018). Potassium isotopic analyses were performed at the Isotope Laboratory of the University of Washington, Seattle, following established procedures (Hu et al., 2018; Xu et al., 2019). In brief, samples and standards were dissolved in a mixture of concentrated HF-HNO_3-HCl acids. Potassium is separated from matrix elements through cation exchange chromatography with Bio-Rad AG 50 W-X8 cation exchange resin (200–400 mesh) in 0.5 N HNO_3 media. The procedure was repeated to obtain pure K solution for mass spectrometry. The K yield is close to 100% and the total procedure blank is <9 ng. The purified K from the sample was introduced into a "cold plasma" via a DSN-100 desolvation system with the RF forward power ranging from 750 to 850 W. The K isotopes were measured by the standard-sample bracketing method using a Nu Plasma II MC-ICPMS. The intensity of ^{40}K was not measured due to isobaric interference of ^{40}Ar. Only ^{39}K and ^{41}K were measured in pseudo high-resolution mode at the interference-free

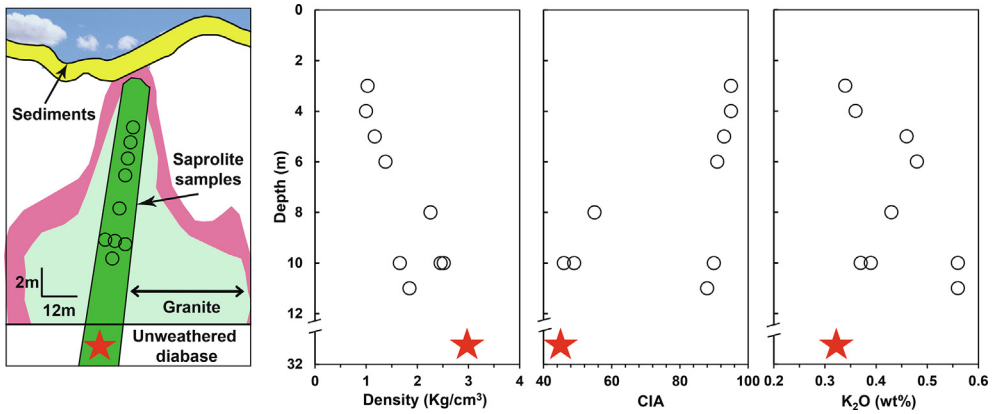

Fig. 3. Sketch of cross-section of the diabase weathering profile (modified from Rudnick et al., 2004) and variations in density, CIA, and K_2O content along the profile, with unweathered diabase at the bottom and increasing degree of weathering upwards. See footnote to Table 1 for definition of CIA.

shoulders of ^{39}K and ^{41}K. The K isotopic data are reported relative to the NIST K standard SRM 3141a (Hu et al., 2018):

$$\delta^{41}K(‰) = \left\{ \frac{(^{41}K/^{39}K)_{sample}}{(^{41}K/^{39}K)_{SRM3141a}} - 1 \right\} \times 1000$$

The long-term external precision, based on replicate analysis of geostandards and seawater samples, is <0.06‰ (95% confidential interval) (Hu et al., 2018). Granite and basalt standards as well as Hawaiian seawater analyzed during the course of this study are within the uncertainty of previously published results (Tables 1–3) (Chen et al., 2019b; Hille et al., 2019; Xu et al., 2019).

4. RESULTS

The unweathered South Carolina diabase has a $\delta^{41}K$ of $-0.475 \pm 0.028‰$. Saprolites developed on the diabase display a narrow range in $\delta^{41}K$ of $-0.462 \pm 0.028‰$ to $-0.396 \pm 0.035‰$ (Fig. 4). By contrast, $\delta^{41}K$ values in the granite weathering profile decrease systematically from $-0.493 \pm 0.030‰$ in unweathered granite samples at the bottom of the drill core to $-0.628 \pm 0.021‰$ in highly-weathered saprolites approaching the surface (Fig. 5).

Stream waters collected near the granite weathering profile display a large range in $\delta^{41}K$ (-0.709 ± 0.017 to $-0.339 \pm 0.018‰$), encompassing the values of relatively unweathered granites and saprolites (Fig. 6). All but one sample (LD-RW20141117) have K isotopic composition similar to or heavier than the unweathered granite. Sample LD-RW20141117 has the lightest K isotopic composition ever reported for river waters (Fig. 6).

5. DISCUSSION

Saprolites developed on the diabase from South Carolina are highly weathered, as indicated by their extremely low density and high CIA values (Fig. 3). However, the K isotopic variation within the weathering profile is limited, barely beyond the analytical uncertainty, and does not correlate with indexes of weathering such as depth and CIA values (Fig. 4). The lack of K isotope fractionation is consistent with the conservative behavior of K during chemical weathering of the diabase. Even though these samples are highly weathered, K content does not change systematically, with τ K_2O (see Table 3 for definition of τ K_2O) varying from −35% to 36%, indicating that some samples lost K while others gained K during weathering (Fig. 4). Therefore, large K isotope fractionation might only occur when a significantly greater amount of K is mobilized during weathering.

By contrast, K isotopes are significantly and systematically fractionated within the granite weathering profile. As inter-mineral K isotope fractionation is limited at magmatic temperatures (<0.06‰, Y.H. Li et al., 2019; Zeng et al., 2019) and K-feldspar is the dominant K-rich mineral in these granites, the observed isotopic variation is unlikely to be produced by preferential leaching of different igneous minerals. Instead, the isotopic fractionation must have been generated during chemical weathering. This is strongly supported by the negative correlations between $\delta^{41}K$ and intensity of chemical weathering, as measured by sample depth, CIA, and kaolinite abundance (Fig. 5). The heavily weathered samples at the top of the profile are enriched in light K isotopes compared to relatively unweathered granites at the bottom, suggesting that light K isotopes are preferentially retained in the weathered regolith relative to fluids. This interpretation is further supported by the variable but overall isotopically heavy K in the stream waters (Fig. 5).

Given the limited fractionation observed in the diabase weathering profile, the discussion below focuses on the factors controlling K isotope fractionation during granite weathering, followed by their implications for global K isotopic mass balance.

5.1. Mechanisms for K isotope fractionation during granite weathering

K-feldspar is the major host of K in the unweathered granites; hence, the behavior of K isotopes during weathering is dominated by the incongruent weathering of K-feldspar, which breaks down to illite, then to kaolinite, accompanied by the release of soluble silica and K cations

Table 1
Potassium isotopic compositions of granite standard G-2, unweathered granites, and saprolite samples from Guangdong, China.

Sample	Depth (m)	K-feldspar (wt. %)	Illite (wt.%)	Kaolinite (wt.%)	Illite/K-feldspar	K_2O (wt.%)	τ K_2O (%)	CIA	$\delta^{41}K$ (‰)	2SD (‰)	95% c.i. (‰)	N
TT-1	1.0	4.2	4.2	57.0	1.00	1.65	−80	90	−0.649	0.060	0.048	4
Replicate									−0.623	0.057	0.024	8
Average									−0.628		0.021	
TT-2	2.0	20.0	9.3	43.6	0.47	3.43	−55	79	−0.599	0.153	0.071	7
TT-3	3.0	18.1	12.1	40.7	0.67	3.51	−43	75	−0.591	0.051	0.024	7
TT-4	4.0	23.7	12.4	35.7	0.52	5.27	−18	63	−0.602	0.106	0.055	6
TT-5	5.0	21.7	12.5	29.6	0.58	4.71	−23	64	−0.597	0.078	0.048	5
TT-6	6.0	16.4	9.5	34.2	0.58	5.24	−18	70	−0.577	0.019	0.012	5
TT-10	10.0	39.1	3.5	25.7	0.09	6.27	−3	68	−0.544	0.088	0.054	5
TT-12-2	12.5	49.9	7.9	21	0.16	7.33	14	65	−0.572	0.072	0.038	6
TT-13-2	13.5	29.1		33.6		5.12	−15	70	−0.586	0.127	0.067	6
TT-14-2	14.5	53.8		25.1		6.51	12	58	−0.572	0.092	0.048	6
TT-16	16.0	55.9	7.3	20.9	0.13	7.56	22	60	−0.508	0.065	0.040	5
TT-17-3	17.7	27.5	12.5	31	0.45	5.76	−14	63	−0.499	0.064	0.033	6
TT-25-3	25.5	57.8	5.4	9.8	0.09	6.50	9	61	−0.525	0.096	0.077	4
TT-27-1	27.0	43.7	9.9	10	0.23	6.83	15	57	−0.548	0.038	0.023	5
TT-28-3	28.5	54.7	5.4	11.3	0.10	6.46	−1	61	−0.516	0.075	0.039	6
TT-29-2	29.3	38.3	8.4	7.7	0.22	5.53	−7	63	−0.527	0.033	0.020	5
TT31-4	31.6	27.6				4.85	−11	53	−0.493	0.057	0.030	6
TT34-4	34.6	37.9				6.45	3	51	−0.506	0.078	0.036	7
TT39-3	39.4	23.8				5.77	−3	48	−0.496	0.098	0.041	8
G-2									−0.448	0.057	0.026	7
Duplicate									−0.448	0.038	0.031	4
Duplicate									−0.461	0.066	0.041	5
Average									−0.450		0.018	

Note 1. To evaluate the relative mobilization of K_2O during weathering, the τ K_2O was used and calculated using the following the equation: $\tau K_2O\ (\%) = 100 \times [(K_2O/Al_2O_3)_i - (K_2O/Al_2O_3)_p]/(K_2O/Al_2O_3)_p$, where $(K_2O/Al_2O_3)_i$ is the ratio of K_2O to Al_2O_3 in weathering products, and $(K_2O/Al_2O_3)_p$ is that in the parent (unweathered) rocks.
Note 2. Chemical index of alteration (CIA) is defined as molar $Al_2O_3/(Al_2O_3 + CaO^* + Na_2O + K_2O)$, where CaO* is the amount of CaO in silicates, which has been used to measure the transformation of feldspar to clay minerals and the degree of chemical weathering (Nesbitt and Young, 1982).
Note 3. 2SD represents two standard deviation; 95% c.i. = 95% confidence interval, represents two standard error corrected by the Student's t factor; N = number of analyses. See Hu et al. (2018) for more details.
Note 4. Replicate represents repeat sample dissolution, column chemistry, and instrumental analysis. Duplicate represents repeat analyses of the same K cut in different instrumental analytical sessions. Average represents error weighted values.
Note 5. Depth, mineral abundance and major elemental data are from Wang et al. (2018).

Table 2
Potassium isotopic compositions of seawater standard and stream water samples from Guangdong, China.

Sample	Sampling date	pH	K (ppm)	Na (ppm)	$\delta^{41}K$ (‰)	2SD (‰)	95% c.i. (‰)	N
LD-RW20140917	09/17/2014	6.83	2.94	4.66	−0.494	0.089	0.040	6
Replicate					−0.451	0.032	0.020	7
Average					−0.460		0.018	
LD-RW20141117	11/17/2014	6.85	3.70	6.11	−0.701	0.001	0.069	2
Replicate					−0.710	0.067	0.018	9
Average					−0.709		0.017	
LD-RW20150117	01/17/2015	6.76	2.71	5.14	−0.458	0.081	0.044	5
Replicate					−0.429	0.082	0.016	8
Average					−0.432		0.015	
LD-RW20150316	03/16/2015	6.67	3.20	6.08	−0.537	0.120	0.049	4
Replicate					−0.457	0.030	0.020	7
Average					−0.468		0.019	
LD-RW20150518	05/18/2015	6.35	2.56	3.91	−0.454	0.047	0.044	5
Replicate					−0.432	0.025	0.017	7
Average					−0.435		0.016	
LD-RW20150727	07/27/2015	6.51	2.54	4.42	−0.424	0.033	0.049	4
Replicate					−0.381	0.067	0.016	8
Average					−0.385		0.015	
LD-RW20150929	09/29/2015	6.51	2.76	4.87	−0.331	0.053	0.049	4
Replicate					−0.340	0.050	0.019	8
Average					−0.339		0.018	
LD-RW20151125	11/25/2015	6.42	2.47	5.16	−0.404	0.110	0.037	7
Replicate					−0.396	0.035	0.017	7
Average					−0.397		0.015	
Seawater					0.136	0.025	0.034	5
Replicate					0.153	0.035	0.022	6
Duplicate					0.134	0.030	0.018	6
Duplicate					0.144	0.043	0.040	6
Average					0.141		0.012	

Note 1. 2SD represents two standard deviation; 95% c.i. = 95% confidence interval, represents two standard error corrected by the Student's t factor; N = number of analyses. See Hu et al. (2018) for more details.
Note 2. Replicate represents repeat sample dissolution, column chemistry, and instrumental analysis. Duplicate represents repeat analyses of the same K cut in different instrumental analytical sessions. Average represents error weighted values.
Note 3. Sampling date, pH, K and Na contents of stream water are from Wang et al. (2018).

into solutions. These reactions can be simplified to the following two steps:

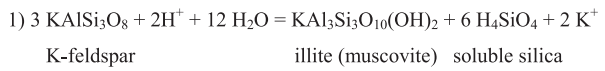

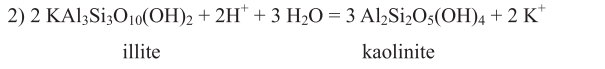

Potassium isotope fractionation can potentially occur (1) between dissolved K^+ and K-bearing minerals in both steps, (2) between different minerals in both steps, and (3) between adsorbed-K in kaolinite and structurally-bound K in illite in step 2. Although the last process is capable of producing large isotope fractionations in some stable isotope systems such as Mg, Cu, and Zn (see reviews of Moynier et al., 2017; Teng, 2017), it is unlikely to be the main cause for the K isotopic variation in the saprolite, as K-feldspar and illite, instead of kaolinite, dominate the K budget even in the most weathered samples. Therefore, the first two processes are likely responsible for fractionating K isotopes during weathering of the granite.

Large isotope fractionation between dissolved K^+ and silicate-hosted K is supported by the overall isotopically heavy stream waters relative to the saprolites (Fig. 5). The one stream sample (LD-RW20141117) with the unusually low $\delta^{41}K$ also has the highest Na and K contents and pH (Fig. 6), which might reflect inheritance of K from the complete dissolution of isotopically light saprolites formed during a more advanced stage of weathering. The mineral dissolution process can be approximated by Rayleigh distillation, with light K isotopes preferring saprolites (e.g., K-feldspar and illite) to waters. The apparent α [$\alpha = (^{41}K/^{39}K)_{saprolite}/(^{41}K/^{39}K)_{fluid}$] values vary from 0.99992 to 0.9996 (Fig. 7), which corresponds to a range of K isotope fractionation between saprolite and fluid from −0.08‰ to −0.4‰. This range in α overlaps with the calculated K isotope fractionation between illite and water (ca. −0.2‰) (Zeng et al., 2019); however, it differs from another theoretical study, which suggests that muscovite is enriched in

Table 3
Potassium isotopic compositions of basalt standard BHVO-1, unweathered diabase (M-20), and saprolite samples from South Carolina, U.S.A.

Sample	Depth (m)	Density (Kg/cm^3)	K_2O (wt.%)	τ K_2O (%)	CIA	$\delta^{41}K$ (‰)	2SD (‰)	95% c.i. (‰)	N
M-7	3.0	1.0	0.34	−35	95	−0.403	0.106	0.025	10
Replicate						−0.417	0.075	0.039	6
Average						−0.407		0.021	
M-8	4.0	1.0	0.36	−32	95	−0.478	0.078	0.040	6
Replicate						−0.446	0.072	0.039	6
Average						−0.462		0.028	
M-9	5.0	1.2	0.46	3	93	−0.427	0.079	0.044	5
M10	6.0	1.4	0.48	2	91	−0.396	0.077	0.035	8
M-12	8.0	2.3	0.43	26	55	−0.450	0.063	0.036	7
M-14	10.0	1.7	0.56	31	90	−0.454	0.075	0.036	7
L14-8	10.0	2.5	0.37	14	49	−0.407	0.082	0.044	7
L14-9	10.0	2.5	0.39	24	46	−0.401	0.075	0.047	6
M-15	11.0	1.9	0.56	36	88	−0.451	0.095	0.044	7
M-20	30.0	3.0	0.32	0	45	−0.459	0.053	0.036	7
Replicate						−0.498	0.067	0.044	7
Average						−0.475		0.028	
BHVO-1						−0.396	0.066	0.032	6
Duplicate						−0.406	0.023	0.044	5
Average						−0.399		0.026	

Note 1. To evaluate the relative mobilization of K_2O during weathering, the τ K_2O was used and calculated by following the equation: τ K_2O (%) = $100 \times [(K_2O/Al_2O_3)_i - (K_2O/Al_2O_3)_p]/(K_2O/Al_2O_3)_p$, where $(K_2O/Al_2O_3)_i$ is the ratio of K_2O to Al_2O_3 in weathering products, and $(K_2O/Al_2O_3)_p$ is that in the parent (unweathered) rocks.
Note 2. Chemical index of alteration (CIA) is defined as molar $Al_2O_3/(Al_2O_3 + CaO^* + Na_2O + K_2O)$, where CaO* is the amount of CaO in silicates, which has been used to measure the transformation of feldspar to clay minerals and the degree of chemical weathering (Nesbitt and Young, 1982).
Note 3. 2SD represents two standard deviation; 95% c.i. = 95% confidence interval, represents two standard error corrected by the Student's t factor; N = number of analyses. See Hu et al. (2018) for more details.
Note 4. Replicate represents repeat sample dissolution, column chemistry, and instrumental analysis. Duplicate represents repeat analyses of the same K cut in different instrumental analytical sessions. Average represents error weighted values.
Note 5. Depth, density and K_2O data are from Gardner et al. (1981).

heavy K isotopes by ~0.5‰ compared to water, while K-feldspar is depleted by ~0.3‰ at room temperature (Y.H. Li et al., 2019).

Our saprolite data suggest that illite is enriched in light K isotopes compared to K-feldspar. This is indicated by the negative trend between $\delta^{41}K$ and the illite/K-feldspar ratio, where more deeply weathered saprolite samples tend to have higher illite/K-feldspar ratios and lower $\delta^{41}K$ values (Fig. 7). To account for the isotopically heavy K in stream waters, mass balance also suggests that illite in the saprolite is enriched in light isotopes relative to K-feldspar in the unweathered granite. Our conclusion is further supported by the recent theoretical calculation suggesting that illite is ~0.3‰ lighter than K-feldspar (Zeng et al., 2019). Nonetheless, the fractionation between illite and K-feldspar suggested here might reflect kinetic processes instead of equilibrium fractionation, considering the sluggishness of isotope exchange at room temperature.

5.2. Implications for K isotope fractionation during chemical weathering

Our study demonstrates that large K isotope fractionation occurs during chemical weathering, with fluids taking heavy K isotopes. This finding has important implications for using K isotope geochemistry to trace continental weathering, ocean chemistry, crustal cycling, and mantle heterogeneity.

The contribution of chemical weathering to global elemental distribution and cycling has been well documented (Berner and Berner, 2012). Our results here suggest that chemical weathering also governs global K isotopic distribution and is the major process that produces the complementary and highly heterogeneous K isotopic compositions of crustal rocks and rivers. Furthermore, our data reveal a strong negative correlation between $\delta^{41}K$ and indexes of chemical weathering, and hence greater K isotopic variation would be expected to occur at extreme weathering conditions. The most weathered sample in the granite weathering profile still contains 1.5 wt.% K_2O after losing ~80% K_2O. As weathering intensifies, the enhanced K loss in the saprolite will lead to an even lighter K isotopic composition. For example, a saprolite sample with a K_2O content of 0.5 wt.% would have a $\delta^{41}K$ value of −0.9‰, assuming a fractionation factor $\alpha = 0.99985$. The highly heterogeneous K isotopic values in weathered products can thus be accounted for by varying degrees of chemical weathering.

The highly variable and commonly heavy K isotopic composition of stream waters studied here is complimentary to the variably light weathered residues resulting from differential weathering. Furthermore, K is biologically

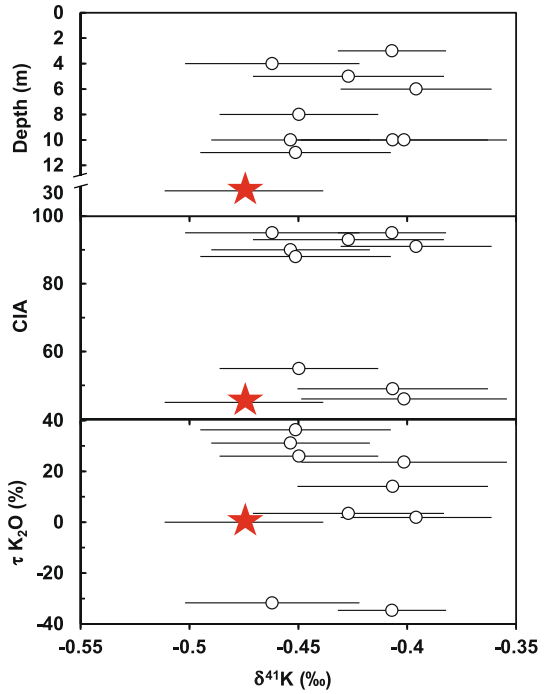

Fig. 4. Plots of $\delta^{41}K$ versus depth, CIA and τ K_2O of saprolites from the diabase weathering profile in South Carolina. See footnote to Table 1 for definition of CIA and τ K_2O. Stars represent unweathered diabase. Error bars in this and the following figure represent 95% confidence interval.

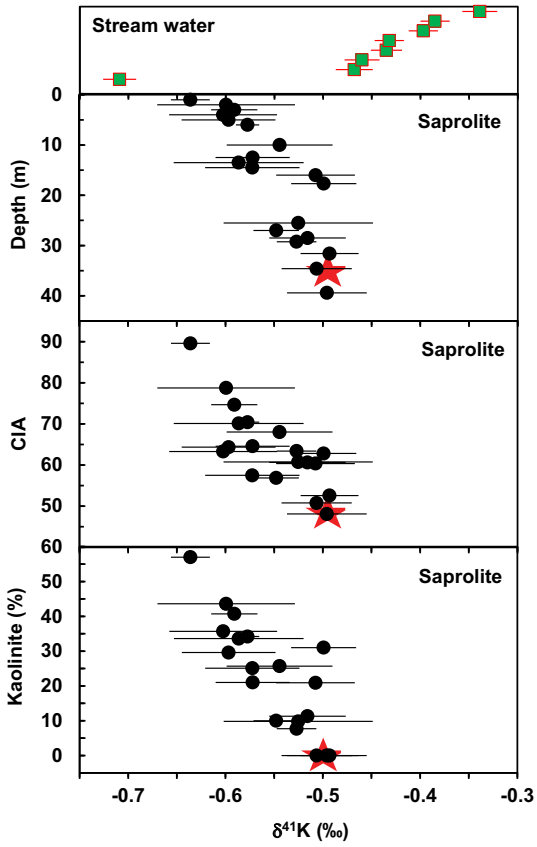

Fig. 5. Potassium isotope fractionation along the granite weathering profile, with progressively lower $\delta^{41}K$ values in more intensely weathered saprolites as indicated by shallower depth, higher CIA and higher kaolinite abundance. Stars represent the average of the relatively unweathered granites. Nearby stream waters are also plotted for comparison. See footnote to Table 1 for definition of CIA.

active and is enriched in plants. Biological processes are expected to play a role in fractionating K isotopes during weathering (Li et al., 2016; Christensen et al., 2018). Thus, chemical weathering, combined with contributions from heterogeneous bedrocks and plants, might be responsible for the large K isotopic variations observed in other rivers (S.L. Li et al., 2019).

Our results also provide insight into the K isotopic balance of the oceans. The average $\delta^{41}K$ of stream samples in our study is lower than that of the seawater. Similar results have also been observed for rivers from other locations (S.L. Li et al., 2019). Hence, the K isotopic composition of seawater is controlled by other processes in addition to the riverine inputs, which are required to either remove light K isotopes from, or add heavy K isotopes to the oceans in order to shift the bulk oceanic $\delta^{41}K$ to the current value of 0.14‰ (Hille et al., 2019). The K elemental budget of the oceans is mainly controlled by inputs from continental runoff (mainly riverine input) and high-temperature hydrothermal activity, and by outputs to low-temperature alteration of seafloor basalts and sediments (reverse weathering, diagenetic K fixation, cation exchange) (Berner and Berner, 2012). Large K isotopic variation has recently been observed in ophiolites and pore fluids (Parendo et al., 2017; Santiago Ramos et al., 2018). These studies indicate that K isotopes are not quantitatively removed from seawater to altered products, and the large K isotope fractionation associated with oceanic sinks might be responsible for balancing the seawater isotopic budget. Thus, secular variations of seawater K isotopic compositions may prove to be a powerful tracer of continental weathering, atmospheric evolution, and hydrothermal activity over geologic time.

Our study, together with recent literature (Parendo et al., 2017; Santiago Ramos et al., 2018; Huang et al., 2020), shows that large K isotope fractionation occurs during water-rock interactions, especially at low temperatures, similar to other stable isotope systems (Valley and Cole, 2001; Teng et al., 2017). These processes result in highly heterogeneous K isotopic distribution in both continental crust (Huang et al., 2020) and subducting slabs. This isotopic heterogeneity, coupled with variable but generally high K concentration in crustal materials, makes K isotopes a powerful tracer of crustal cycling in the mantle (e.g., Sun et al., 2020).

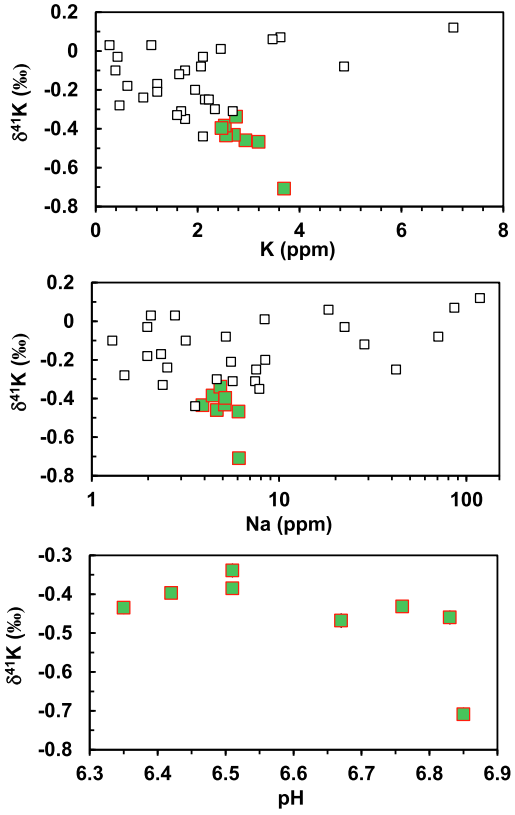

Fig. 6. Potassium isotopic variation versus water compositions (K, Na and pH) for nearby streams measured in this study (filled squares) and rivers from the literature (open squares) (S.L. Li et al., 2019).

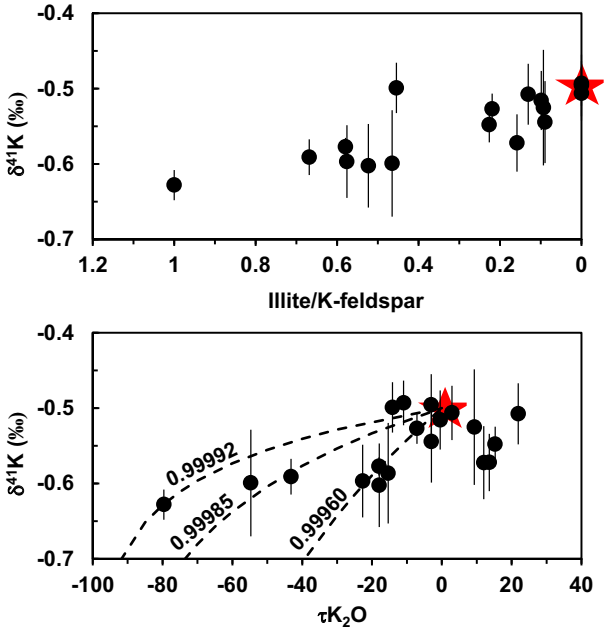

Fig. 7. Plots of $\delta^{41}K$ versus illite/K-feldspar (top panel) and versus τ K_2O (bottom panel). Dotted lines in the bottom panel depict K removal via Rayleigh distillation for different values of the fractionation factor α $[=(^{41}K/^{39}K)_{saprolite}/(^{41}K/^{39}K)_{fluid}]$. Stars represent the average of the relatively unweathered granites.

6. CONCLUSIONS

High-precision K isotopic data for saprolites developed on diabase and granite weathering profiles, as well as data from local stream waters, lead to the following conclusions:

1. Saprolites from the diabase weathering profile are heavily weathered, but display limited K isotopic variation, which mainly reflects the conservative behavior of K during diabase weathering, with >50% of the original K remaining in the saprolites.
2. Saprolites from the granite weathering profile show significant and systematic K isotope fractionation (~0.15‰). Nearby stream waters display a slightly larger range (~0.37‰) in $\delta^{41}K$.
3. The large variation in $\delta^{41}K$ in the granitic saprolites results from isotope fractionation during chemical weathering, as indicated by the negative correlation between $\delta^{41}K$ with various indexes of weathering (e.g., sample depth, CIA, and kaolinite abundance).
4. Light K isotopes partition into weathered residues relative to fluids, as supported by the isotopically light saprolites and overall isotopically heavy stream water samples.
5. Continental weathering fractionates K isotopes significantly and is thus one of the main processes producing highly heterogeneous rivers and crustal rocks.
6. Large K isotope fractionation produced by fluid-rock interactions at Earth's surface, coupled with variably high K contents in surface materials, makes K isotopes a potentially powerful tracer of crustal recycling into the mantle.

Declaration of Competing Interest

The authors declare that they have no known competing financial interests or personal relationships that could have appeared to influence the work reported in this paper.

ACKNOWLEDGEMENTS

FZT is grateful to Roberta L. Rudnick for her great mentorship throughout his PhD studies and her continuous encouragement and inspiration since then.

We thank Xin-Yang Chen, Tian-Yi Huang and Nicolas Dauphas for helpful discussions, and three anonymous reviewers for insightful and critical comments. The diabase weathering profile samples were originally provided by the late Bob Gardner. The careful and efficient editorial handing by AE Prof. Brian Stewart and EE Prof. Jeff Catalano is greatly appreciated.

APPENDIX A. SUPPLEMENTARY MATERIAL

Supplementary data to this article can be found online at https://doi.org/10.1016/j.gca.2020.02.029.

REFERENCES

Berner E. K. and Berner R. A. (2012) *Global Environment: Water, Air and Geochemical Cycles*. Princeton University Publisher, 488 pp.

Brantley S. L., Megonigal J. P., Scatena F. N., Balogh-Brunstad Z., Barnes R. T., Bruns M. A., Van Cappellen P., Dontsova K., Hartnett H. E., Hartshorn A. S., Heimsath A., Herndon E., Jin L., Keller C. K., Leake J. R., McDowell W. H., Meinzer F. C., Mozdzer T. J., Petsch S., Pett-Ridge J., Pregitzer K. S., Raymond P. A., Riebe C. S., Shumaker K., Sutton-Grier A., Walter R. and Yoo K. (2011) Twelve testable hypotheses on the geobiology of weathering. *Geobiology* **9**(2), 140–165.

Chen H., Meshik A. P., Pravdivtseva O. V., Day J. M. D. and Wang K. (2019a) Potassium isotope fractionation during high-temperature evaporation determined from the Trinity nuclear test. *Chem. Geol.* **522**, 84–92.

Chen H., Tian Z., Tuller-Ross B., Korotev R. L. and Wang K. (2019b) High-precision potassium isotopic analysis by MC-ICP-MS: an inter-laboratory comparison and refined K atomic weight. *J. Anal. At. Spectrom.* **34**(1), 160–171.

Christensen J. N., Qin L., Brown S. T. and DePaolo D. J. (2018) Potassium and calcium isotopic fractionation by plants (soybean [Glycine max], rice [oryza sativa], and wheat [triticum aestivum]). *ACS Earth Space Chem.* **2**, 745–752.

Gaillardet J., Dupre B., Louvat P. and Allegre C. J. (1999) Global silicate weathering and CO2 consumption rates deduced from the chemistry of large rivers. *Chem. Geol.* **159**(1–4), 3–30.

Gardner L. R. and Kheoruenromne I. (1980) Siderite veins in saprolite, Cayce, South Carolina. South Carolina. *Geology* **24** (1), 29–31.

Gardner L. R., Kheoruenromne I. and Chen H. S. (1981) Geochemistry and mineralogy of an unusual diabase saprolite near Columbia, South Carolina. *Clays Clay Miner.* **29**(3), 184–190.

Goldich S. S. (1938) A study in rock weathering. *J. Geol.* **46**, 17–58.

Hille M., Hu Y., Huang T.-Y. and Teng F.-Z. (2019) Homogeneous and heavy potassium isotopic composition of global oceans. *Sci. Bullet.* **64**, 1740–1742.

Hu Y., Chen X.-Y., Xu Y.-K. and Teng F.-Z. (2018) High-precision analysis of potassium isotopes by HR-MC-ICPMS. *Chem. Geol.* **493**, 100–108.

Huang T.-Y., Teng F.-Z., Rudnick R. L., Chen X.-Y., Hu Y., Liu Y.-S. and Wu F.-Y. (2020) Heterogeneous potassium isotopic composition of the upper continental crust. *Geochimica et Cosmochimica Acta* **278**, 122–136.

Li S. L., Li W. Q., Beard B. L., Raymo M. E., Wang X. M., Chen Y. and Chen J. (2019) K isotopes as a tracer for continental weathering and geological K cycling. *Proc. Natl. Acad. Sci. United States America* **116**(18), 8740–8745.

Li W., Beard B. L. and Li S. (2016) Precise measurement of stable potassium isotope ratios using a single focusing collision cell multi-collector ICP-MS. *J. Anal. At. Spectrom.* **31**, 1023–1029.

Li W., Kwon K. D., Li S. L. and Beard B. L. (2017) Potassium isotope fractionation between K-salts and saturated aqueous solutions at room temperature: Laboratory experiments and theoretical calculations. *Geochim. Cosmochim. Acta* **214**, 1–13.

Li Y. H., Wang W. Z., Wu Z. Q. and Huang S. C. (2019) First-principles investigation of equilibrium K isotope fractionation among K-bearing minerals. *Geochim. Cosmochim. Acta* **264**, 30–42.

Liu S.-A., Teng F.-Z., Li S., Wei G.-J., Ma J.-L. and Li D. (2014) Copper and iron isotope fractionation during weathering and pedogenesis: Insights from saprolite profiles. *Geochim. Cosmochim. Acta* **146**, 59–75.

Morgan L. E., Ramos D. P. S., Davidheiser-Kroll B., Faithfull J., Lloyd N. S., Ellam R. M. and Higgins J. A. (2018) High-precision $^{41}K/^{39}K$ measurements by MC-ICP-MS indicate terrestrial variability of $\delta^{41}K$. *J. Anal. At. Spectrom.* **33**(2), 175–186.

Moynier F., Vance D., Fujii T. and Savage P. S. (2017) The isotope geochemistry of zinc and copper. *Rev. Mineral. Geochem.* **82**, 543–600.

Nesbitt H. W. and Young G. M. (1982) Early Proterozoic climates and plate motions inferred from major element chemistry of lutites. *Nature* **299**, 715–717.

Parendo C. A., Jacobsen S. B. and Wang K. (2017) K isotopes as a tracer of seafloor hydrothermal alteration. *Proc. Natl. Acad. Sci. United States America* **114**, 1827–1831.

Penniston-Dorland S., Liu X.-M. and Rudnick R. L. (2017) Lithium isotope geochemistry. *Rev. Mineral. Geochem.* **82**, 165–217.

Rudnick R. L. and Gao S. (2003) Composition of the continental crust. In *The Crust* (ed. R. L. Rudnick). Treatise on Geochemistry, Elsevier-Pergamon, Oxford, pp. 1–64.

Rudnick R. L., Tomascak P. B., Njo H. B. and Gardner L. R. (2004) Extreme lithium isotopic fractionation during continental weathering revealed in saprolites from South Carolina. *Chem. Geol.* **212**(1–2), 45–57.

Santiago Ramos D. P., Morgan L. E., Lloyd N. S. and Higgins J. A. (2018) Reverse weathering in marine sediments and the geochemical cycle of potassium in seawater: Insights from the K isotopic composition ($^{41}K/^{39}K$) of deep-sea pore-fluids. *Geochim. Cosmochim. Acta* **236**, 99–120.

Sun Y., Teng F.-Z., Hu Y., Chen X.-Y. and Pang K.-N. (2020) Tracing subducted oceanic slabs in the mantle by using potassium isotopes. *Geochimica et Cosmochimica Acta* **278**, 353–360.

Teng F.-Z., Li W.-Y., Rudnick R. L. and Gardner L. R. (2010) Contrasting behavior of lithium and magnesium isotope fractionation during continental weathering. *Earth Planet. Sci. Lett.* **300**, 63–71.

Teng F.-Z., Watkins J. M. and Dauphas N. (2017) Non-traditional stable isotopes. In *Riviews in Mineralogy & Geochemistry*, vol. 82, p. 885. Riviews in Mineralogy & Geochemistry. Mineralogical Society of America and the Geochemical Soceity, Washington, D. C..

Teng F.-Z. (2017) Magnesium isotope geochemistry. *Rev. Mineral. Geochem.* **82**, 219–287.

Teng F.-Z., Wang S.-J. and Moynier F. (2019) Tracing the formation and differentiation of the Earth by non-traditional stable isotopes. *Sci. China Earth Sci.* **62**, 1702–1715.

Tuller-Ross B., Marty B., Chen H., Kelley K. A., Lee H. and Wang K. (2019) Potassium isotope systematics of oceanic basalts. *Geochim. Cosmochim. Acta* **259**, 144–154.

Valley J. W. and Cole D. R. (2001) Stable isotope geochemistry. In *Reviews in Mineralogy & Geochemistry*, vol. 43663, p. pp. Reviews in Mineralogy & Geochemistry. Mineralogical Society of America and the Geochemical Soceity, Washington D. C.

Wang K. and Jacobsen S. B. (2016a) An estimate of the Bulk Silicate Earth potassium isotopic composition based on MC-ICPMS measurements of basalts. *Geochim. Cosmochim. Acta* **178**, 223–232.

Wang K. and Jacobsen S. B. (2016b) Potassium isotopic evidence for a high-energy giant impact origin of the Moon. *Nature* **538**, 487–490.

Wang Z., Ma J., Li J., Wei G., Zeng T., Li L., Zhang L., Deng W., Xie L. and Liu Z. (2018) Fe (hydro) oxide controls Mo isotope fractionation during the weathering of granite. *Geochim. Cosmochim. Acta* **226**, 1–17.

Wedepohl K. H. (1995) The composition of the continental crust. *Geochim. Cosmochim. Acta* **59**(7), 1217–1232.

Xu Y. K., Hu Y., Chen X. Y., Huang T. Y., Sletten R. S., Zhu D. and Teng F. Z. (2019) Potassium isotopic compositions of international geological reference materials. *Chem. Geol.* **513**, 101–107.

Zeng H., Rozsa V., Nie N. X., Zhang Z., Pham T. A., Galli G. and Dauphas N. (2019) Ab Initio calculation of equilibrium isotopic fractionations of potassium and rubidium in minerals and water. *ACS Earth Space Chem.*. https://doi.org/10.1021/acsearthspacechem.9b00180.

Associate editor: Brian W. Stewart